Statics and kinetics of the ordering transition in the $AuAgZn_2$ alloy

Frédéric Livet,* Françoise Bley,† and Jean-Paul Simon‡
Laboratoire de Thermodynamique et de Physico-Chimie Métallurgique (UMR CNRS 5614), ENSEEG-INPG, BP 75, 38402 Saint Martin D'Hères, France

René Caudron§
ONERA, 29Av. Div. Leclerc, 92320 Chatillon, France and LLB, CNRS-CEA, CE Saclay, 91190 Gif sur Yvette, France

Jacques Mainville‖ and Mark Sutton¶
Physics Department, McGill University, Montreal, Québec, Canada H3A 2T8

David Lebolloc'h**
LPS, Bât. 510, Univ. Paris Sud, 91405 Orsay, France

(Received 19 April 2002; revised manuscript received 18 July 2002; published 31 October 2002)

The Heusler order-disorder transition in the $AuAgZn_2$ alloy is studied by x-ray scattering using the D2AM beamline at the ESRF. The static critical fluctuations above T_c are measured and are shown to follow Ising-like behavior. *In situ* kinetics of ordering are studied at T_Q after quenching from T_c+5 °C. For $T_Q<T_c-2$ °C, the growth of ordered domains is shown to have a $t^{1/2}$ dependence. For temperatures closer to T_c, the influence of critical fluctuations on the kinetics is discussed. First, the time increase of the fluctuations after quench above T_c is observed. The T_Q and q dependence of the process is discussed from a dynamical scaling hypothesis. For $T_c>T_Q>T_c-2$ °C, the main observation in the vicinity of T_c is the observation of an *incubation time* before the normal $t^{1/2}$ domain growth. These experiments provide direct observations of the critical slowing down in a critical system with a nonconserved order parameter.

DOI: 10.1103/PhysRevB.66.134108 PACS number(s): 64.60.Ht, 05.70.Jk, 61.10.Eq, 05.70.Fh

I. INTRODUCTION

Ordering transitions in crystalline alloys based on the bcc structure are excellent model systems for the observation of critical fluctuations. In the case of ''Heusler'' alloys, like $Au_{1+x}Ag_{1-x}Zn_2$, two main transitions can be observed[1]: an $A2$-$B2$ transition (of CsCl structure, like CuZn) and an Heusler transition, similar to the $B2$-DO_3 transition observed in Fe_3Al.[2–4] This corresponds to antiferromagnetic ordering on a simple cubic (sc) lattice, a sc to face-centered cubic (fcc) transition.

Transitions in these systems are usually second order. Coupling between multiple order parameters, like in the 25% concentration range for the Fe_3Al alloy,[5–7] can lead to a first-order transition. From symmetry arguments, the transitions belong to the Ising universality class.

For $x=0$, the $AuAgZn_2$ alloy is $B2$ ordered from the liquid,[8,9] and the $B2$-DO_3 transition is observed close to 330 °C.[8] Measuring the $[\frac{1}{2}\frac{1}{2}\frac{1}{2}]$ Bragg superstructure peak is a direct way to study this transition ($Q_0=(2\pi/a)[\frac{1}{2}\frac{1}{2}\frac{1}{2}]$, $a=3.17$ Å (Ref. 9) being the lattice parameter of the $B2$ structure). In some cases, coupling to the order parameter of an elastic field can change the behavior close to the transition temperature T_c. Only careful study in the vicinity of the transition can check that the transition is continuous.

A principal interest in these ordering transitions is that their dynamics is equivalent to an ''Ising model with nonconserved order parameter'' (model A in Ref. 10). For ordering transitions, the order parameter $\eta(r)$ corresponds to the difference in site occupation, and the elementary spin-flip process corresponds to the interchange of Au and Ag atoms on sc lattice sites.

At low temperatures, the system orders, and the dynamics of ordering has been discussed by Allen and Cahn.[11,12] From thermodynamic arguments, the increase of the average size of the domains L can be written

$$L^2=Dt, \tag{1}$$

where we have introduced D which, far from T_c, corresponds to the diffusion constant.

For temperatures close to T_c ($\epsilon=|T-T_c|/T_c$), the thermodynamics is dominated by fluctuations. The correlation length ξ and the corresponding fluctuation time τ diverge close to T_c with critical exponents defined as

$$\xi\simeq\alpha_0\epsilon^{-\nu}, \tag{2}$$

$$\tau\simeq\alpha_1\epsilon^{-z\nu}. \tag{3}$$

The dynamic exponent z should differ from γ/ν only by a small amount for three dimensions.[13,14]

In this paper, the time-, temperature-, and q-dependent diffuse intensity $S(q,\epsilon,t)$ is measured. For an instantaneous quench from infinite temperature, the dynamical scaling hypothesis, given a scaling transform of $q\rightarrow bq$, assumes

$$S(q,\epsilon,t)=b^{\gamma/\nu}S(qb,\epsilon b^{1/\nu},tb^{-z}). \tag{4}$$

From this scaling form one can obtain the limiting behavior for various cases of interest by the appropriate choice of b.

To get the limiting temperature dependence of the peak height ($q=0$) choosing $b=\epsilon^{-\nu}$ gives

$$S(0,\epsilon,t)=\epsilon^{-\gamma}S(0,1,t\epsilon^{\nu z}). \quad (5)$$

In practice, $q=0$ means $q\ll\xi^{-1}$. For nonzero ϵ and infinite t, the equilibrium dependence obtained is

$$S(0,\epsilon,\infty)=\epsilon^{-\gamma}S(0,1,\infty), \quad (6)$$

giving the usual critical exponent for the susceptibility. In practice, this requires that $t\gg\tau$.

To obtain the wave vector dependence near T_c, choose $b=q^{-1}$ in Eq. (4). With $\epsilon=0$ $[\epsilon\ll(q\alpha_0)^{1/\nu}]$ and infinite t $[t\gg\alpha_1(\alpha_0 q)^z]$, the static critical scattering scales as

$$S(q,0,\infty)=q^{-\gamma/\nu}S(1,0,\infty). \quad (7)$$

Finally, the time dependence follows from choosing $b=t^{1/z}$ to give

$$S(q,\epsilon,t)=t^{\gamma/\nu z}S(qt^{1/z},\epsilon t^{1/\nu z},1). \quad (8)$$

One assumes that $S(x,y,1)$ has a finite limit for $x=0$ and $y=0$. Under the conditions $t\ll\alpha_1/(\alpha_0 q)^z$ and $t\ll\alpha_1\epsilon^{-z\nu}$, the establishment of fluctuations is approximatively q and ϵ independent:

$$S(q,\epsilon,t)\simeq t^{\gamma/\nu z}S(0,0,1). \quad (9)$$

In these universal equations, the constants α_0 and α_1 are dependent on the system under study and on the way ξ and τ are defined from experiment.

In this work, we report *in situ* measurements carried out with the D2AM instrument at the ESRF (European synchrotron at Grenoble, France) on $AuAgZn_2$ single crystals. First, precise static measurements provide direct evidence of the second-order character of the transition. Static results provide an important starting point for understanding the critical dynamics of our system. Then the kinetics of ordering is studied by using temperature quenches where the sample is aged at T_a and quenched to T_Q. Three different regions of temperatures are distinguished: deep quenches $T_Q\ll T_c$, where the usual $t^{1/2}$ [Eq. (1)] domain increase is verified, quenches close to but above T_c to study critical fluctuations in the disordered phase, and quenches close to but below T_c to study critical fluctuations and ordering in the ordered phase.

II. DESCRIPTION OF THE EXPERIMENTS

A. Beam

The D2AM (BM2) beamline is located on an ESRF bending magnet source. Monochromatization is achieved by means of a Si(111) double monochromator, $\lambda\simeq1.55$ Å, and the wavelength resolution is

$$\frac{\Delta\lambda}{\lambda}=1.36\times10^{-4}. \quad (10)$$

The second monochromator is bent, to focus horizontally at the sample position, 9 m away. Two horizontal symmetric mirrors on both sides of the monochromators are used for vertical focusing. The first one is bent to make the beam parallel during monochromatization, and the second one is bent to focus the beam vertically at the sample position (see Ref. 15). Two different resolutions were used.

(1) For the static experiment, a 3×3 mm^2 [vertical $\times$horizontal $(V\times H)$] beam size has been selected in the optics hutch, with a 110×130 μm^2 [full width at half maximum (FWHM) $V\times H$] focal spot, with a beam intensity of the order of 3×10^9 photons/s.

(2) For the dynamics measurement, the beam size was decreased to 0.8×0.8 mm^2, and by carefully selecting the regions on the mirrors, a focal spot of 70×125 μm^2 (FWHM, $V\times H$) was obtained, with a beam intensity 10 time lower.

The x-ray intensity corresponds to a power of microwatts and thus leads to negligible local heating of the sample.

B. Sample preparation and environment

A cylindrical 3-cm-long single crystal was obtained. A $\langle111\rangle$ axis is close to the cylindrical axis, and the $AuAgZn_2$ samples were cut parallel to the (111) face and carefully polished. In order to limit surface contamination and Zn evaporation, a 10-nm-thick Al layer was deposited, which provides after heating an alumina coating. A Bragg reflection geometry was used, and the diffraction plane was vertical. For the two experiments described here, water-cooled vacuum furnaces were developed, each with a high long-term stability of about ±0.02 °C in the 280–365 °C temperature range. Improvements in quench rates and in absolute temperature measurements were made between the two measurements reported here. In the quench experiment the maximum cooling rate was 2 °C/s, but in order to avoid temperature oscillations, much slower quenches were used.

C. Detection

A direct-illumination charge-coupled-device (DI-CCD) area detector was used. In this type of detector, x rays are directly converted to electronic charges at the surface of the Si-based CCD.[16] As these charges are significantly larger than those introduced by electronic noise, one can locate individual x rays by frequent reading of the detector and identifying in each frame the absorbed x rays (''droplets'') with an on-line computer program (see Ref. 17). The spatial resolution of the detector is one pixel (22×22 μm^2) and the detector is 384×576 pixels in area. The overall detection quantum efficiency at 8 keV is 51%. The droplet algorithm was designed for count rates less than 0.1 x ray per pixel, but works well enough for count rates up to 1 x ray per pixel for small regions. In these experiments, either the static diffuse intensity or the time evolution of the scattered intensity after a quench close to the Bragg peak is measured for which the intensity is usually strongly peaked. With the 430 kHz analog-to-digital converter (ADC) used, the minimum reading time was 0.57 s for a full frame. A fast shutter controlled the exposure time, which varied between 0.5 s and 0.1 s. For a static experiment, the whole detector was used, and some hundreds of frames were measured before being treated by our program. In the second case, the time evolution of the sample was followed *in situ* by means of 500–2000 frames

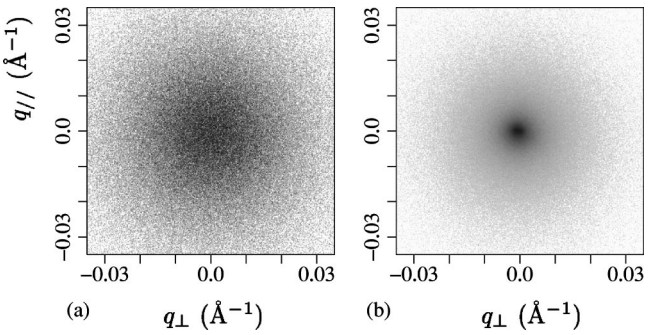

FIG. 1. Diffuse scattering intensity observed at 355 °C (T_c +4 °C) and 351.15 °C (T_c+0.13 °C). Areas of only 300×300 pixels (22×22 μm^2 at 0.37 m) are plotted. The $q_\perp$ direction is perpendicular to Q_0. A logarithmic gray scale is used with the minimum value of 10 and the maximum values of 60 and 4000 (counts per 100 s per pixel) for (a) and (b), respectively.

in a limited region (200×200 pixels). Each frame was measured for 0.1–2 s, depending on intensities, with a 0.146 s dead time for each reduced frame. The maximum measured scattered intensity was limited to values lower than a few tenths of x ray per pixel per frame by means of Cu attenuators.

D. Resolution

For low-resolution (static) experiments the sample to detector distance was 0.37 m; for high resolution (kinetics) this distance was 1.26 m. In both experiments, the resolution is determined by the size of the beam at the sample and by the angular spread of the converging beam. The predicted experimental resolution is 1.4×1.6 $(10^{-3}$ Å$^{-1})^2$ (FWHM, $H\times V$) for low resolution and 0.5×0.6 $(10^{-3}$ Å$^{-1})^2$ (FWHM, $H\times V$) for high resolution. Even with this high resolution, our experiments are far from being coherent: the product of the resolution by the size of the irradiated region (10^6 Å) is much larger than unity.

III. STATIC RESULTS

A. Typical scattering observed

After alignment, the sample was heated to 355 °C and then slowly cooled close to T_c. The strongly peaked diffuse intensity was used to align the scattering vector with the $[\frac{1}{2}\frac{1}{2}\frac{1}{2}]$ superstructure Bragg peak. The static critical scattering was then precisely measured.

Figure 1 shows an example of the measured intensity I at 355 and 351.15 °C (T_c+4 °C and T_c+0.13 °C) from the central part of the detector (about 4×4 mm^2 at 0.37 m) obtained from 500 and 1000 frames of 0.1 s, respectively. Frames were summed after "droplet" analysis.[17] Critical scattering in the vicinity of the superstructure position is isotropic, as expected in a system dominated by Ising critical fluctuations.

Large variations in intensity can be observed by this method as electronic noise is suppressed, enabling quite low counting rates to be observed. This is shown in Fig. 2, where the diffuse intensity has been averaged over pixels belonging

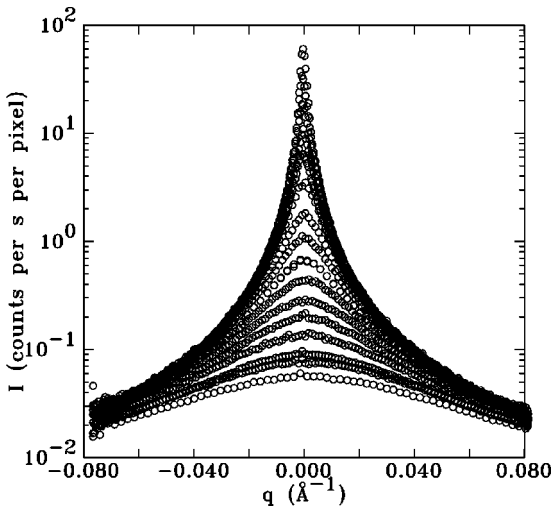

FIG. 2. Critical scattering at temperatures varying from 365 °C (T_c+14 °C) to 351.1 °C (T_c+0.08 °C) along the $q_\parallel$ direction, after sector averaging of the CCD camera.

to the same $q=|\vec{Q}-\vec{Q}_0|$. These rings of scattering were averaged separately over two $\pi/2$ arcs of the detector; the arc for $|\vec{Q}|>Q_0$ is plotted on the right of the figure and the arc for $|\vec{Q}|<Q_0$ on the left.

All results of Fig. 2 have been obtained during a long series of measurements (about 10 h), the equilibration of the sample was carefully checked, and all experiments have been corrected for incident beam variations. Though the resulting $S(q,\epsilon)$ are not normalized to an absolute scale, comparisons for different runs on the same sample can be done.

B. Comparison with the Ising model

From curves like Fig. 2, the value of the maximum intensity S_0 and the FWHM Δq_0 can be estimated. The correlation length ξ_0 is defined by $\xi_0=2/\Delta q_0$. In this figure, the largest fluctuations are observed for $T=351.1$ °C (T_c +0.08 °C): $\Delta q_0\simeq 0.0028$ Å^{-1}, i.e., $\xi\approx 700$ Å. This is twice experimental resolution.

From Eqs. (6) and (2), $S_0^{-1/\gamma}$ and $\xi_0^{-1/\nu}$ should have a linear temperature dependence. In Fig. 3 our results agree well with the generally accepted value $\gamma=1.24$, but $\nu=0.7$ fits better than $\nu=0.63$. Error bars are of the order of the size of dots. This disagreement with the usual exponents corre-

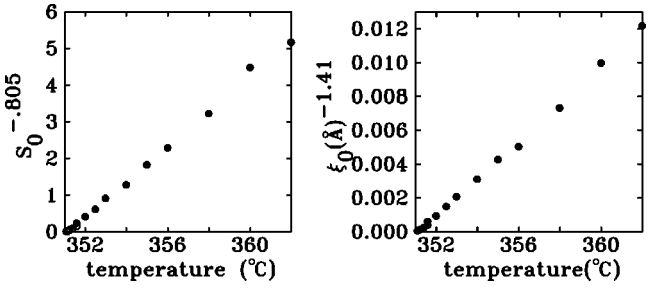

FIG. 3. Linear temperature dependence of $S_0^{-1/\gamma}$ and $\xi_0^{-1/\nu}$ showing nearly Ising behavior, with $T_c=351.02$ °C, $\gamma=1.24$, and $\nu=0.7$.

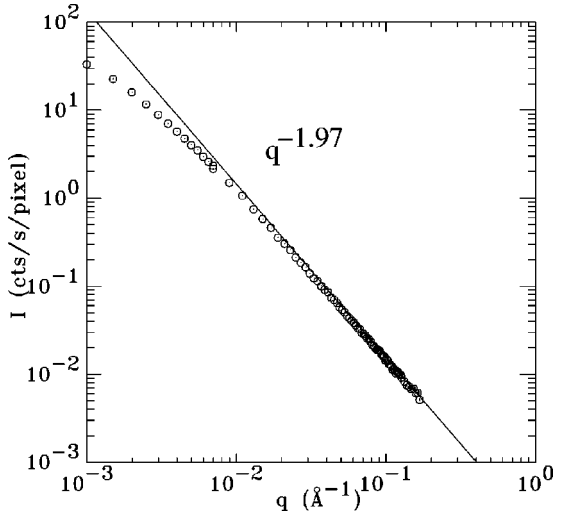

FIG. 4. Critical fluctuations at 351.1 °C. The log-log plot shows a trend towards $q^{-\gamma/\nu}$ behavior (the solid line uses $\gamma/\nu=1.97$).

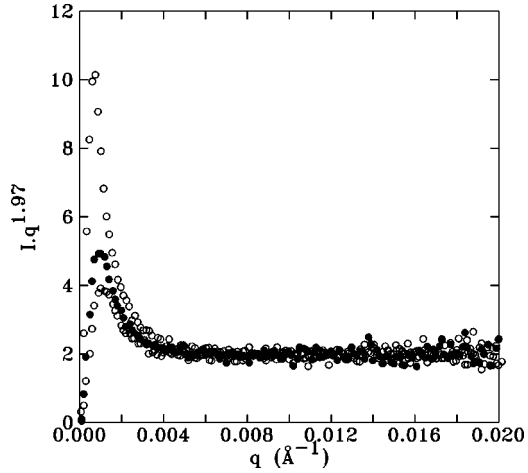

FIG. 5. Plot of $q^{1.97}I(q)$ (scale arbitrary) showing critical scattering in the large-q region below T_c. Isotropic average of three different temperatures: $T_c-0.07$ °C, $T_c-0.12$ °C, and $T_c-0.22$ °C.

sponding to the Ising model is small. The transition temperature is estimated to 351.02(2) °C in this experiment. If a $\nu=0.63$ value is assumed and only the $\epsilon<0.002$ data are used, the fluctuation length ξ_0, as deduced from Δq_0, can be written

$$\xi_0=2.5\ \epsilon^{-0.63}\ (\text{Å}). \tag{11}$$

These figures clearly show that the transition is second order and that the system does not have mean-field behavior ($\gamma=1, \nu=0.5$).

In order to discuss the q variation of the critical scattering [Eq. (7)], measurements were carried out at $T=351.1$ °C with nine different positions of the detector, covering a 2θ range of $\pm 1.6°$. The intensities plotted in Fig. 4 include the results of these nine measurements. They have been corrected for incident beam intensity changes and for angular variations of x-ray absorption. An asymmetric Compton scattering term was also subtracted. With our photon-counting algorithm, the diffuse scattering intensity is obtained covering four orders of magnitudes, and the statistical errors are small because lower intensities are averaged over thousands of pixels. The main remaining systematic errors are difficult to estimate. The asymptotic behavior, with $\gamma/\nu=1.97$, is only observed for large values of q ($q\xi_0 \geqslant 10$, with $\xi_0=700$ Å). In this case, a fit for Eq. (7) in the q range from 0.011 Å^{-1} to 0.17 Å^{-1} (i.e., $q\xi=8$ to $q\xi=120$) gives $\gamma/\nu=1.95\pm0.02$. If lower q values are taken into account, this ratio is apparently smaller, which agrees well with the higher value of $\nu=0.7$ observed in Fig. 3. Though critical exponents are difficult to measure precisely, the behavior is close to that predicted by the Ising model.

Below T_c, after aging about 10 min, domain sizes were large, and Bragg peaks become resolution limited. Very close to T_c, Bragg peaks and diffuse scattering are simultaneously observed, as shown in Fig. 5, where the measured intensities have been multiplied by $q^{1.97}$, and plotted versus q for three temperatures: 350.95, 350.9, and 350.8 °C, i.e., $T_c-0.07$ °C, $T_c-0.12$ °C, and $T_c-0.22$ °C. The constant limit of these plots for $q>4.\times10^{-3}$ Å^{-1} corresponds to critical scattering of fluctuations in the ordered phase. For lower q values the Bragg peaks show an increase of intensities for decreasing temperatures.

IV. KINETICS

Based on the static results, improvements in the heat transfer of the furnace and in diffraction resolution were deemed necessary for the kinetics studies. In the improved furnace, the measured critical temperature was about 13 °C lower, mainly resulting from reduced temperature gradients between the heater and sample.

A. Quenches

The sample was repeatedly quenched from $T_a=344$ °C ($T_c+5.6$ °C). In order to compensate for thermal lattice expansion, the sample was first oriented at the quench temperature T_Q, then heated again to T_a. A temperature quench consisting of several short and small temperature jumps was used to reduce undercooling induced by the temperature controller. Measurements of the diffracted intensity were started at the end of the quench. The area of the CCD camera used was limited to 200×200 pixels for faster readout times. With the sample to detector distance of 1.26 m, $|q|\leqslant10^{-2}$ Å^{-1}. The sample temperature was simultaneously measured with a $\simeq0.01$ °C precision. In all cases, no change in the position of maximum intensity was observed after sample had reached T_Q, indicating that lattice parameter does not change during ordering.

B. Deep quenches

For large temperature changes ($T_c \gg T_Q$), quench rates in the vicinity of the critical temperature are about 1.0 °C s^{-1}, and the measurements are started when the final temperature is reached within ±1 °C, which is 35–45 s after the beginning of the quench.

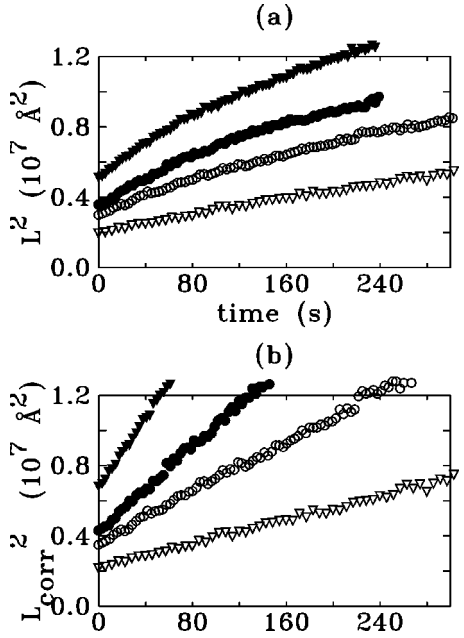

FIG. 6. Time evolution of the domain sizes L^2 as observed after quenches to 280 °C ($T_c-58.37$ °C), 300 °C ($T_c-38.37$ °C), 310 °C ($T_c-28.37$ °C), and 320 °C ($T_c-18.37$ °C) (from lower to upper curves) without (a) and with (b) deconvolution corrections.

Far from T_c, the diffuse scattering intensity can be neglected. The size of domains can be estimated from the first moment of the intensity distribution:

$$L(t)=\int I(q,t)d^2q \Big/ \int |q|I(q,t)d^2q. \tag{12}$$

Measured intensities vary by about six orders of magnitude in the detector area. In practice, integrals in Eq. (12) are evaluated in the region where intensity is larger than 10^{-3} of its maximum. L corresponds to the average domain size. From previous studies, a $t^{1/2}$ behavior is expected for the size increase. Figure 6(a) shows L^2 versus time for four different temperatures: 280 °C ($T_c-58.37$ °C), 300 °C ($T_c-38.37$ °C), 310 °C ($T_c-28.37$ °C), and 320 °C ($T_c-18.37$ °C). In this plot, one observes that in the initial state, the domain size is large: a few thousand Å. Except for the lowest temperature, curves are far from linear, and this is explained by the finite resolution of the setup used. In Fig. 6(b), estimated L from Eq. (12) have been corrected for experimental smearing ($\Delta q=2.2\times10^{-4}$ Å^{-1}) by the simplified deconvolution formula

$$L_{corr}^{-2}=L^{-2}-\Delta q^2. \tag{13}$$

This value of Δq corresponds roughly to three pixels in our CCD camera. If the beam is considered as Gaussian distributed, the experimental FWHM is $4\sqrt{\ln 2/\pi}\Delta q\simeq4.1\times10^{-4}$ Å^{-1} and is close to the expected resolution. From Fig. 6(b), where L^2 is approximately linear in time, an estimate of D in Eq. (1) can be obtained. An Arrhenius plot of the variations of $\ln(D)$ versus $1/T$ is shown in Fig. 7, and an approximate temperature variation of D can be deduced:

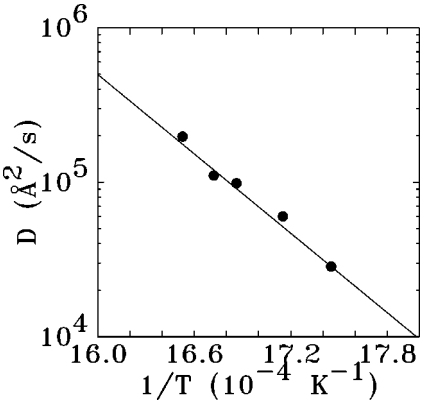

FIG. 7. Arrhenius plot of the temperature dependence of D below T_c. The line corresponds to Eq. (14).

$$D=D_0\exp(-E_a/k_BT), \tag{14}$$

where $D_0\simeq2500$ cm^2/s and $E_a\simeq1.7$ eV correspond to the straight line in Fig. 7.

C. Quenches above T_c

In order to observe the kinetics of the establishment of short-range order above T_c, it is very important to limit undercooling during a quench. If the temperature is lower than T_c, even for a short time, the observed kinetics is strongly modified. For this reason, a more complex heat treatment was done. The sample was quenched from 344 °C in several steps to T_Q taking a total of 45 s, and the time spent in the range from T_Q+1 °C to T_Q was about 15 s. Data taking was started at $T_Q+0.05$ °C and the undershoot was less than 0.1 °C, and lasted only a few seconds.

Figure 8 shows the shape of the scattering obtained in this sample at 338.5 °C ($T_c+0.13$ °C), in the vicinity of T_c, in the very central part of the detector. Besides the diffuse intensity corresponding to critical fluctuations, small sharp peaks were observed. These peaks are treated as parasitic, probably due to microscopic crystallites of different composition at the surface As this structure was stable during the

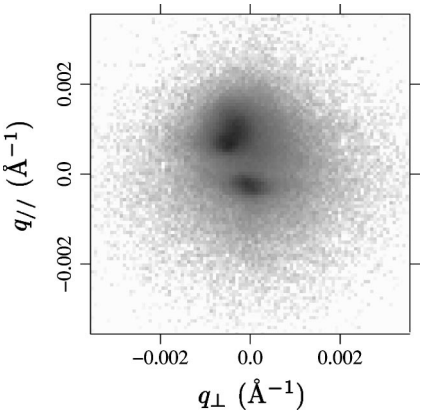

FIG. 8. Observation of parasitic peaks in the central part of the CCD detector at 338.5 °C ($T_c+0.13$ °C). Corresponding pixels are discarded during data analysis.

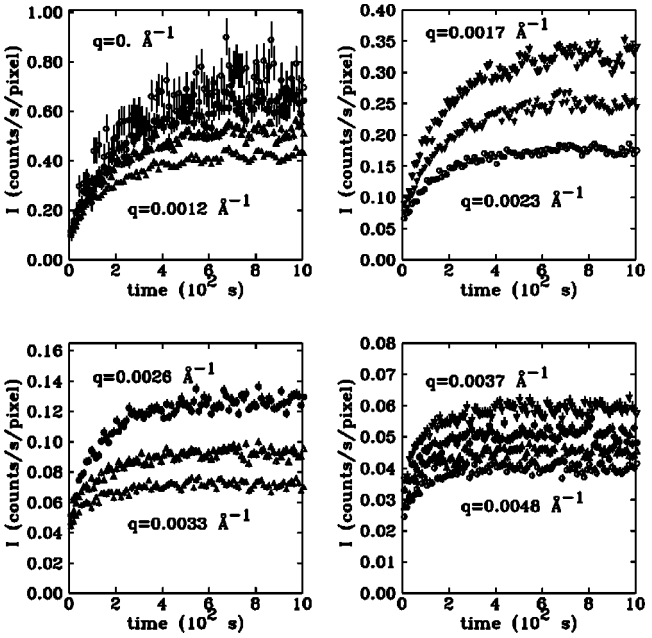

FIG. 9. Time evolution of the diffuse intensities for various q values at 338.45 °C ($T_c+0.08$ °C) (q increments of 3.5×10^{-4} Å^{-1} are used between curves).

two days of measurement, pixels corresponding to these peaks were discarded from the analysis of the diffuse scattering.

Apart from these small regions, intensities are symmetric, as was observed in the static measurements (see Fig. 1). Intensities are grouped into rings of constant $|q|$ which are several pixels wide to obtain $I(q,\epsilon,t)$. These are corrected for incident beam intensity variations, and results nominally correspond to counts per pixel per second. Figure 9 shows typical curves obtained at 338.45 °C ($T_c+0.08$ °C). The width of the ring is five pixels ($\delta q=0.351\times10^{-3}$ Å^{-1}). Because of the elimination of the parasitic peaks, error bars are large for the central part of the detector ($q\simeq0$). Within the time of measurement, large increases of diffuse intensities can be observed. Comparing intensities at different wave vectors q's shows that the larger the wave vector, the faster is the intensity change. For $q<2.3\times10^{-3}$ Å^{-1} the intensity is still varying during the last 500 s. One can also notice some oscillations in intensities, of period about 120 s, which are related to small (less than 0.02 °C) temperature oscillations. After 1000 s, the system can be considered as roughly in equilibrium. If the correlation length ξ_0 is calculated from $I(q,\epsilon,t=\infty)$, one obtains $\xi_0=660$ Å, which, from our static results [Eq. (11)], corresponds to $T_c+0.08$ °C. In the new oven, $T_c=338.37(2)$ °C.

The temperature variations of the time evolution for a given q ($q=1.2\times10^{-3}$ Å^{-1}) are shown in Fig. 10. For temperatures close to T_c (from 338.55 to 338.4 °C), intensities for $t<60$ s are similar. This corresponds to the small-q and short-time behavior predicted from Eq. (9). At long times, a difference by a factor of 2 is observed. After about 8 min, the intensity at 338.4 °C ($T_c+0.03$ °C) seems to be still increasing, even though it is also oscillating due to small temperature instabilities. These curves do not scale, but in these data

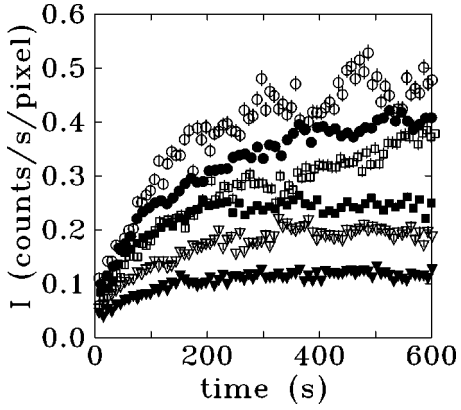

FIG. 10. Time evolution of intensities for $q=1.2\times10^{-3}$ Å^{-1} at 338.8 °C ($T_c+0.43$ °C) (solid triangles), 338.7 °C ($T_c+0.33$ °C) (open triangles), 338.55 °C ($T_c+0.18$ °C) (solid squares), 338.5 °C ($T_c+0.13$ °C) (open squares), 338.45 °C ($T_c+0.07$ °C) (solid circles), and 338.4 °C ($T_c+0.03$ °C) (open circles).

the product $q\xi_0$ only varies [see Eq. (11)] between 0.3 and 1.6 and so the $\epsilon=0$ condition of Eq. (2) is not fulfilled.

Results of Fig. 11 have been obtained for $q=0$ after elimination of the two parasitic peaks of Fig. 8 and by averaging diffuse intensity over a region of ten pixels radius ($\delta q=0.7\times10^{-3}$ Å^{-1}). For the set of temperatures of this figure, $\xi_0<500$ Å, and the product $\xi_0\delta q$ is small. For short times ($t<100$ s) and close enough to T_c ($T-T_c<0.33$ K), $S(q=0,\epsilon,t)$ is nearly temperature independent, as discussed in the Introduction [Eq. (9)]. From these data $S_\infty=S(q=0,\epsilon,t=\infty)$ has been estimated, and they roughly increase like $\epsilon^{-\gamma}$. They also give a tentative rescaled curve shown in Fig. 12 where $S(q=0,\epsilon,t)/S_\infty$ has been plotted versus t/S_∞. On doing this, one has assumed that $z=\gamma/\nu$ for the sake of simplicity and because these curves cannot provide a more precise estimate of z. This plot shows direct evidence of a critical slowing down and that the larger fluctuations have longer fluctuation times.

The dynamic exponent can be also be obtained by estimating the exponent $\gamma/\nu z$ [Eq. (9)] from the short-time be-

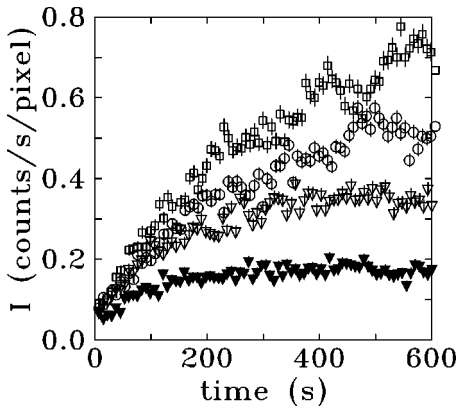

FIG. 11. Time evolution of $S(q=0,\epsilon,t)$ for 338.5 °C ($T_c+0.13$ °C) (squares), 338.6 °C ($T_c+0.23$ °C) (circles), 338.7 °C ($T_c+0.33$ °C) (open triangles), and 338.8 °C ($T_c+0.43$ °C) (solid triangles).

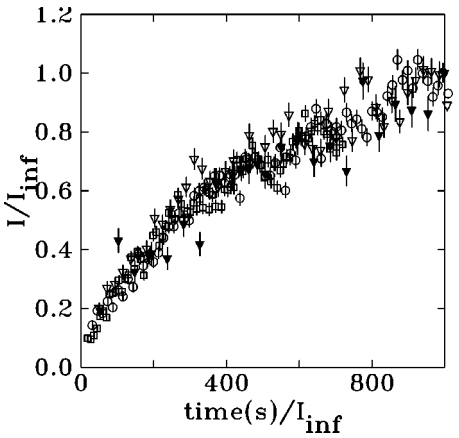

FIG. 12. Elementary renormalization of the time dependent $S(q=0,\epsilon,t)$. A 10 s constant time has been added to correct from the slow quenches. Intensity and time are divided by I_{inf}, an estimate of S_∞ from Fig. 11: 0.9 for 338.5 °C ($T_c+0.13$ °C), 0.55 for 338.6 °C ($T_c+0.23$ °C), 0.36 for 338.7 °C ($T_c+0.33$ °C), and 0.18 for 338.8 °C ($T_c+0.43$ °C).

havior of intensity. This equation is valid for a quench of infinite rate from an infinite temperature and these conditions are far from being fulfilled. Figure 13 shows the data for $T=338.37$ °C (T_cC), i.e., the closest set to T_c. For short time ($t<120$ s), the slope of the log-log plot gives $\gamma/\nu z\simeq 0.9$, i.e., $z\simeq 2.2$. This result is interesting but not very reliable, due to poor statistics, imperfect quenches (a 15 s offset in time has been added), and temperature instabilities.

D. Shallow quenches under T_c

For T_Q close to, but lower than T_c, some diffuse intensity is also observed. Measured intensities after 45 s aging at $T=338$ °C ($T_c-0.37$ °C), 337 °C ($T_c-1.37$ °C), and 336 °C ($T_c-2.37$ °C) are plotted in Fig. 14(a). Intensities vary by about five orders of magnitude. In Fig. 14(b), $I(q)q^{1.97}$ is plotted in order to enhance the critical scattering contribution. In the case of $T=338$ °C ($T_c-0.37$ °C), for large q

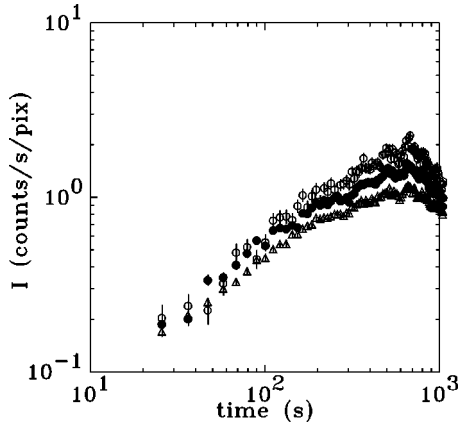

FIG. 13. Time dependence of $S(q,0,t)$ at T_c (338.37 °C) for $q=0$ (open circles), $q=0.5\times10^{-3}$ Å^{-1} (solid circles), and $q=0.9\times10^{-3}$ Å^{-1} (triangles). Log-log plot: the diagonal of the figure (slope 1) corresponds to $z=2$.

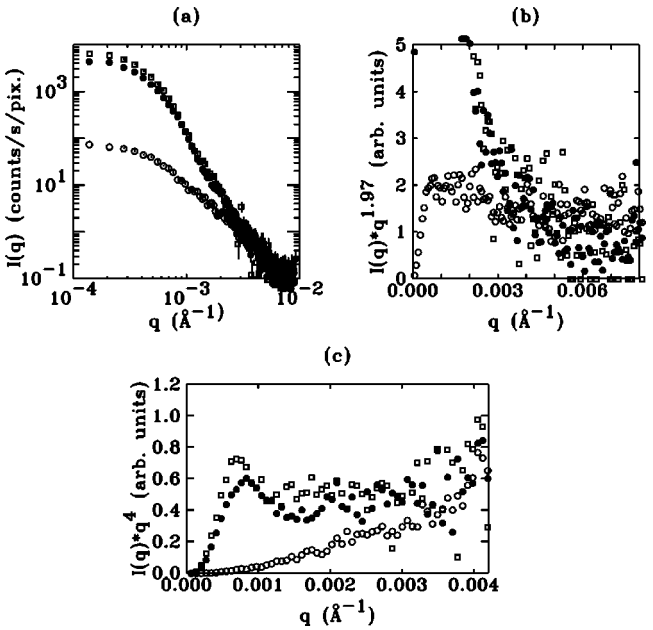

FIG. 14. Intensities observed 45 s after quenching to 338 °C ($T_c-0.37$ °C) (open circles), 337 °C ($T_c-1.37$ °C) (solid circles), and 336 °C ($T_c-2.37$ °C) (open squares). In (b), the intensity is mainly due to critical fluctuations for $q>4.\times10^{-3}$ Å^{-1}, and in (c) one observes a q^{-4} behavior for the two lower temperatures.

($q>4.\times10^{-3}$ Å^{-1}) and for short times ($t<45$ s), one sees that scattering is essentially due to critical fluctuations. In Fig. 14(c), a plot of $I(q)q^4$ shows that for lower temperatures, a constant behavior is observed at intermediate q values. This q^{-4} behavior (Porod's law[18]) shows that antiphase boundaries are present. In small-angle experiments, the observed oscillation (here at $q=8.\times10^{-4}$ Å^{-1}) around Porod's law is interpreted as evidence of curved boundaries.[19,20]

The integrated intensity $I_Q=\int|q|I(q)d^2q$ and the moment in Eq. (12) from the data are shown in Fig. 15 for various temperatures under T_c. For short times, an increase of I_Q is interpreted as evidence of a delay in the establishment of order (from simple arguments, $I_Q\propto\eta^2$, where η is the order parameter).

This increase is observed for short time ($t<50$ s) at all temperatures, except for the two closest to T_c, where the determination of I_Q cannot be considered reliable (no definite interfaces) during the first 1 or 2 min. At these temperatures [Fig. 15(b)], the size of the domains remains negligibly small for about 60 s, after which they increase. During this period, the observed intensities are essentially diffuse, and only critical fluctuations are present in our sample, as in Fig. 14(b) (open circles). We interpret this as an ''incubation time'' in this second-order transition. This appears to be the time in which the short-range fluctuations change from their prequench values to ones reflecting the quench temperature values, before the system starts forming domains of the ordered phase. We estimate this time τ_0 to be about 100 s at 338.1 °C ($T_c-0.27$ °C), 70 s at 338 °C ($T_c-0.37$ °C), and 30 s at 337.8 °C ($T_c-0.57$ °C). As our quench rates are low, τ_0 is difficult to estimate precisely. For instance, in Fig. 15, the $t=0$ state of the $T=336$ °C measurement has a nonzero

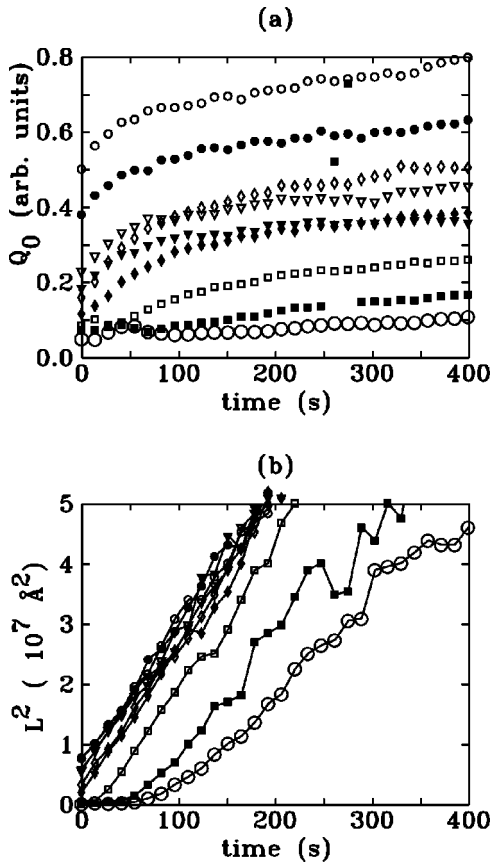

FIG. 15. Time evolution for temperatures close to T_c of (a) the integrated intensity (Q_0) and (b) corrected domain sizes (L_0). Temperatures: open dots, 336 °C ($T_c-2.37$ °C); solid dots, 336.5 °C ($T_c-1.87$ °C); open triangles, 337 °C ($T_c-1.37$ °C); solid triangles, 337.2 °C ($T_c-1.27$ °C); open diamonds, 337.4 °C ($T_c-1.97$ °C); solid diamonds, 337.6 °C ($T_c-0.77$ °C); open squares, 337.8 °C ($T_c-0.37$ °C); solid squares, 338 °C ($T_c-0.37$ °C); circles, 338.1 °C ($T_c-0.27$ °C).

initial L, not surprisingly as the sample has spent about 20 s under T_c before measurements were started. This time τ_0 is the analog of the fluctuation time τ [Eq. (3)] observed above T_c and has the same order of magnitude. If the long-time linear slope of Fig. 15(b) is used for calculating D by Eq. (1), some decrease of D when approaching T_c is observed. At 336 °C, $D\simeq 2.5\times 10^5$ Å^2/s, and at 338 °C, $D\simeq 1.8\times 10^5$ Å^2/s. Comfortably these estimates are close to that from Eq. (14) (2.2×10^5 Å^2/s) but the large deconvolution correction from Eq. (13) gives a large systematic error.

E. From criticality to ordering

In order to illustrate the change which occurs when the quench temperature is lowered from above to below T_c, the kinetics of the system in a very narrow region around T_c is plotted in Fig. 16. In these data, no pixels are discarded, and the width of rings on the CCD camera was two pixels ($\delta q = 1.4\times 10^{-4}$ Å^{-1}). For the highest temperature of this figure ($T_c+0.03$ °C), the system has no long-range order, and the observed structure corresponds to the parasitic peaks of Fig. 8. At this temperature, intensities have the same order of magnitude as the critical scattering. For the three other temperatures, an explosive increase of intensity is observed. Only in the latter results [338.1 °C ($T_c-0.27$ °C)] are domains unambiguously observed with a Porod tail appearing after 150 s (see Fig. 15). In the vicinity of T_c, the dynamics of ordering has a very fast "burst" propagation which is extremely sensitive to the small temperature oscillations of our setup. This also emphasizes why a careful quench process needs to be used in order to limit undershoots close to T_c.

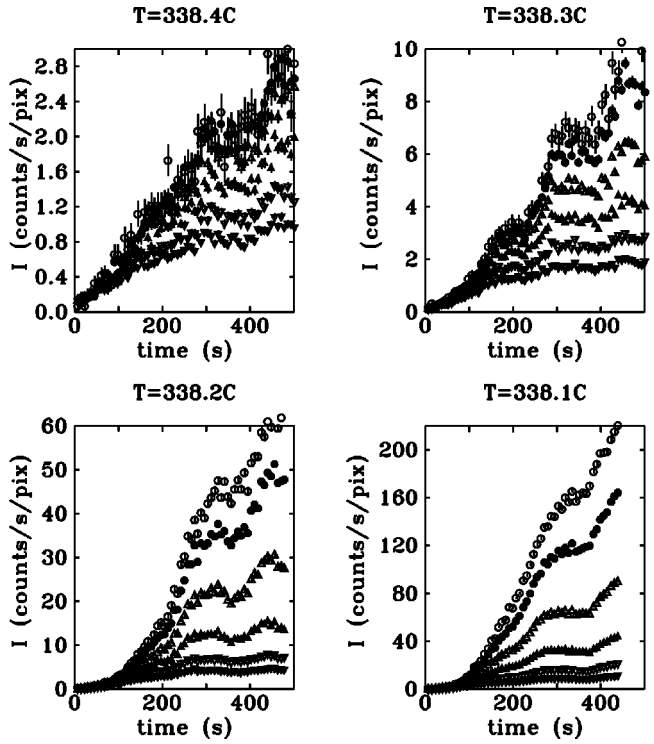

FIG. 16. Intensities (same units as in Fig. 9, 10, and 11) vs time for q varying from 0 to 8×10^{-4} Å^{-1}. Kinetics obtained from crossing the critical point (from $T_c+0.03$ °C to $T_c-0.27$ °C). Resolution and increments used are $\delta q\simeq 1.4\times 10^{-5}$ Å^{-1}.

V. DISCUSSION

Within the precision of our results, this system is compatible with the Ising static universality class. Ordering kinetics, such as studied here, provides good model systems for studying the critical dynamics in nonconserved order parameter systems. Also, there are only a few direct experimental measurements for critical slowing down (see also Ref. 21). A promising new method for studying the dynamics of critical fluctuations in equilibrium is "x-ray intensity fluctuation spectroscopy."[22,23] Indeed, we have started to make such measurements on this system.

The $AuAgZn_2$ system behaves like an Ising critical system. The time scales for critical fluctuations increase as the transition point is approached. Moreover, this slowing down can be observed on both sides of the transition. Below T_c, well-defined antiphase boundaries only occur after some time delay. Our static results provide an estimate of α_0

$\simeq$2.5 Å [Eq. (2)]. This is close to the usual values in critical systems and in the high-temperature limit ($\epsilon \simeq 1$) is on the order of the interatomic distance.

Our dynamics measurements also provide an estimate of the time scales for the establishment of critical fluctuations above and below T_c. From our results of a few degrees below T_c, the time for ordered domains to reach a size of 0.1 μm is about 5 s ($D \simeq 2.4 \times 10^5$ Å^2/s). For comparison, closer to T_c, the time for the correlation length to reach $\simeq 0.1$ μm is on the order of 100 s (see Fig. 10).

Our results can also be used to estimate α_1 by Eq. (3). Defining τ as the half completion time observed from Fig. 11 gives $\tau \simeq 200$ s at $T = 338.5\,^{\circ}$C, i.e., $\epsilon = 0.2 \times 10^{-3}$. Assuming $z=2$, $\alpha_1 = 4. \times 10^{-3}$ s. Another estimate of the time for atomic motion is obtained from a simple model using the diffusion constant $D \simeq 2.2 \times 10^5$ Å^2/s. The time to diffuse 3.2 Å (the distance between two neighboring simple cubic sites) is 40 μs. This is two orders of magnitude faster than our estimate of α_1, probably indicating that the diffusion mechanism is more complicated than simple jumps. It is hard to imagine that this discrepancy can be due to errors in the critical exponents used in the estimation of α_1.

We are in the process of improving our determination of the dynamical exponent z. Improvements are possible by making more rapid quenching profiles and the beamline has been improved, giving an increased incident beam intensity and higher resolution.

ACKNOWLEDGMENTS

The authors want to thank Jean-Francois Bérar, Bernard Caillot, and Stephan Arnault for their support on the D2AM (French CRG) beamline at the ESRF and A. Hammersley for providing the fit2d program.

*Electronic address: flivet@ltpcm.inpg.fr
†Electronic address: fbley@ltpcm.inpg.fr
‡Electronic address: jpsimon@ltpcm.inpg.fr
§Electronic address: caudron@onera.fr
‖Electronic address: Jacques.Mainville@frodo.physics.mcgill.ca
¶Electronic address: mark@frodo.physics.mcgill.ca
**Electronic address: lebolloch@lps.u-psud.fr

[1] A. Prince, *Ternary Alloys: A Comprehensive Compendium of Evaluated Constitutional Data and Phase Diagrams*, edited by G. Petzow and G. Effenberg (VCH, 1988), Vol. 1, pp. 270–278.
[2] P.M.P. Morgand and G. Sainfort, Acta Metall. **16**, 867 (1968).
[3] H. Okamoto and P.A. Beck, Metall. Trans. A **2**, 569 (1971).
[4] A. Taylor and R.M. Jones, J. Phys. Chem. Solids **6**, 16 (1958).
[5] S.M. Allen and J.W. Cahn, Acta Metall. **23**, 1017 (1975).
[6] S.M. Allen and J.W. Cahn, Scr. Metall. **10**, 451 (1976).
[7] F. Schmid and K. Binder, J. Phys.: Condens. Matter **4**, 3569 (1992).
[8] M.E. Brookes and R.W. Smith, Scr. Metall. **3**, 667 (1969).
[9] B. Muldawer, J. Appl. Phys. **37**, 2062 (1966).
[10] P.C. Hohenberg and B.I. Halperin, Rev. Mod. Phys. **49**, 435 (1977).
[11] S.M. Allen and J.W. Cahn, Acta Metall. **24**, 425 (1976).
[12] S.M. Allen and J.W. Cahn, Acta Metall. **27**, 1085 (1979).
[13] B. Halperin, P. Hohenberg, and S.-K. Ma, Phys. Rev. Lett. **29**, 1548 (1972).
[14] C.D. Dominicis, E. Brézin, and J. Zinn-Justin, Phys. Rev. B **12**, 4945 (1975).
[15] J. Simon, E. Geissler, A. Hecht, F. Bley, F. Livet, M. Roth, J.L. Ferrer, E. Fanchon, C. Cohen-Addad, and J.C. Thierry, Rev. Sci. Instrum. **63**, 1051 (1992).
[16] G. Charpak and F. Sauli, *Experimental Techniques in High Energy Physics*, Frontiers in Physics (Addison-Wesley, Reading, MA, 1987), pp. 244–249.
[17] F. Livet, F. Bley, R. Caudron, E. Gessler, D. Abernathy, G. Gruebel, S.G.J.M. Mochrie, M. Sutton, and J. Mainville, Nucl. Instrum. Methods Phys. Res. A **451**, 596 (2000).
[18] F. Bley *et al.*, Acta Crystallogr., Sect. A: Found. Crystallogr. **51**, 746 (1995).
[19] J. Méring and D. Tchoubar, J. Appl. Crystallogr. **1**, 153 (1968).
[20] D. Tchoubar and J. Méring, J. Appl. Crystallogr. **2**, 128 (1969).
[21] B. Park, G.B. Stephenson, S.M. Allen, and K.F. Ludwig, Phys. Rev. Lett. **68**, 1742 (1992).
[22] M. Sutton, S.E. Nagler, S.G. Mochrie, T. Greystak, L.E. Bermann, G. Held, and G.B. Stephenson, Nature (London) **352**, 608 (1991).
[23] S. Brauer, G.B. Stephenson, M. Sutton, R. Brüning, E. Dufresne, S.G.J. Mochrie, G. Grübel, J. Als-Nielsen, and D.L. Abernathy, Phys. Rev. Lett. **74**, 2010 (1995).